Correlated mixtures of adiabatic and isocurvature cosmological perturbations

David Langlois and Alain Riazuelo
Département d'Astrophysique Relativiste et de Cosmologie, Centre National de la Recherche Scientifique, Observatoire de Paris, 92195 Meudon Cedex, France
(Received 23 December 1999; published 19 July 2000)

We examine the consequences of the existence of correlated mixtures of adiabatic and isocurvature perturbations on the CMB and large scale structure. In particular, we consider the four types of ''elementary'' totally correlated hybrid initial conditions, where only one of the four matter species (photons, baryons, neutrinos, CDM) deviates from adiabaticity. We then study the height and position of the acoustic peaks with respect to the large angular scale plateau as a function of the isocurvature to adiabatic ratio.

PACS number(s): 98.80.Cq, 98.70.Vc

I. INTRODUCTION

In the near future, a lot of data about the anisotropies of the cosmic microwave background (CMB) will be available to cosmologists, notably thanks to balloon experiments and the planned satellites, the Microwave Anisotropy Probe (MAP) [1] and Planck [2]. What will be remarkable is the expected high resolution and sensitivity of these experiments, which may turn cosmology into a high precision activity.

One of the hopes of cosmologists is to be able to determine from these data the cosmological parameters describing the geometry and matter contents of our universe. In this respect, it is important to stress that the fluctuations that are and that will be measured result, according to our current understanding, from a *combination of primordial perturbations and cosmological parameters*. In the preparation of future data analysis, one should be careful to avoid oversimplification *a priori* of the primordial perturbations and to not stick to the simplest one-scalar field inflation model. After all, the early universe is the period in the history of the universe where the physics is the least known.

A more general description of the primordial perturbations may therefore be needed to be able to interpret future data. In this perspective, the aim of this work is to examine the consequences of the existence of isocurvature perturbations in addition to the usual adiabatic perturbations. Such studies have already been performed in the case of *independent* mixtures of adiabatic and isocurvature perturbations [3–9]. This is why we will focus our attention on *correlated* mixtures of adiabatic and isocurvature perturbations. The possibility of such primordial perturbations is motivated by the recent work of one of us, which showed that the simplest model of multiple inflation, a model with two massive noninteracting scalar fields, can produce such correlated mixtures [10].

Isocurvature perturbations are perturbations in the relative density ratio between various species in the early universe, in contrast with the more standard adiabatic (or isentropic) perturbations which are perturbations in the total energy density with fixed particle number ratios. Primordial isocurvature perturbations are often ignored in inflationary models. The main reason for this is that they are less universal than adiabatic perturbations because, on the one hand, they can be produced only in multiple inflationary models [11] and, on the other hand, they do not necessarily survive until the present epoch.

However, isocurvature perturbations have been shown to be of potential importance in some specific models: axions [4,5,7,12], Affleck-Dine baryogenesis mechanism [13], multiple field inflation [10,11,14,15].

A priori, since the (not too early) universe is filled with four species, baryons, photons, neutrinos, and dark matter (which will be assumed to be cold here), several types of isocurvature perturbations can be envisaged. For example, in the past, a model with isocurvature baryon perturbations was proposed [16], although it does not seem compatible with the data today [17]. Most recent models, however, contain cold dark matter (CDM) isocurvature perturbations. A more general approach, including neutrino isocurvature perturbations (and also isocurvature velocity perturbations), was considered recently [18]. In the present work, we will focus our attention, for simplicity, on primordial perturbations where only one species deviates from adiabaticity, which thus leaves room to four types of hybrid (i.e., adiabatic plus isocurvature) initial perturbations. These four ''elementary'' modes will be systematically studied, without trying to make any connection with specific early universe models.

As far as observational constraints are concerned, it has already been established that a pure isocurvature scale-invariant spectrum must be rejected because it predicts on large scales too large temperature anisotropies with respect to density fluctuations [12], but other possibilities have been envisaged, like tilted isocurvature perturbations. The main trend, however, has been to study models with a mixing of isocurvature and adiabatic perturbations. Confrontation of these models with observational data, such as CMB anisotropies and large scale structures, seems to allow only for a small fraction of isocurvature perturbations. Future CMB measurements will also enable us to put much tighter constraints on this kind of model.

It must be emphasized, however, that all these studies assumed *independent* mixing of isocurvature and adiabatic perturbations. While this assumption can be indeed justified in some specific early universe models, it is certainly not an absolute rule, as has been shown in [10]. It is thus the purpose of this paper to investigate the consequences on observational quantities, namely, the large scale structure and the

CMB anisotropies, of *correlated mixtures of isocurvature and adiabatic* perturbations. As will be shown, correlation gives more richness to hybrid perturbations. For example, while the first acoustic peak (relatively to the plateau) is always lower for independent hybrid perturbations than for pure adiabatic perturbations, it can be either lower or higher with correlated hybrid perturbations.

The plan of the paper will be the following. In the next section (Sec. II), we recall the basic definitions of isocurvature and adiabatic perturbations and introduce hybrid perturbations. Then, Sec. III will discuss the notion of correlation between isocurvature and adiabatic perturbations. In Sec. IV, we will begin the systematic analysis of the correlated hybrid perturbations by considering the long wavelength modes, which can be solved analytically. Section V is devoted to the numerical investigation for all cosmological scales. Finally, we present our conclusions in Sec. VI. There is also an appendix, which details the evolution equations and gives the full solution for the long wavelength modes.

II. ADIABATIC AND ISOCURVATURE PERTURBATIONS

In this section, we will define precisely the notion of adiabatic and isocurvature perturbations, and introduce the notation that will be used throughout this paper. Only perturbations of the scalar type will be considered here.

The perturbations of the spacetime geometry will be described by two scalar potentials Φ and Ψ, which appear in the linear perturbation of the (flat) Friedmann-Lemaître-Robertson-Walker (FLRW) metric,

$$ds^2 = -a^2(\eta)(1+2\Phi)\mathrm{d}\eta^2 + a^2(\eta)(1-2\Psi)\delta_{ij}\mathrm{d}x^i\mathrm{d}x^j, \tag{1}$$

a choice which corresponds to the longitudinal gauge (η is the conformal time and δ_{ij} is the Kronecker symbol).

For matter, we will consider four different species: two relativistic species, photons and massless neutrinos; two nonrelativistic species, baryons and CDM. Their respective energy density contrasts will be denoted δ_γ, δ_ν, δ_b, and δ_c ($\delta_A \equiv \delta\rho_A/\rho_A$).

Before defining adiabatic and isocurvature perturbations, let us introduce the idea of entropy perturbation, which can be defined for any pair of components A and B by the expression

$$S_{A,B} \equiv \frac{\delta n_A}{n_A} - \frac{\delta n_B}{n_B}, \tag{2}$$

where n_A represents the particle number density for the species A. When the equation of state for a given species is such that $w \equiv p/\rho = \text{const}$, then one can reexpress the entropy perturbation in terms of the density contrast in the form

$$S_{A,B} \equiv \frac{\delta_A}{1+w_A} - \frac{\delta_B}{1+w_B}. \tag{3}$$

By definition, an adiabatic (or isentropic) perturbation corresponds to the case where all the entropy perturbations are zero. For our four components, this can be expressed as

$$\delta_c = \delta_b = \frac{3}{4}\delta_\nu = \frac{3}{4}\delta_\gamma \equiv \delta_{(a)}, \tag{4}$$

where $\delta_{(a)}$ will denote the common value (up to the adiabatic index of the equation of state) of the density contrasts. An adiabatic perturbation is thus characterized by a unique amplitude, which can be $\delta_{(a)}$ but which is usually given, for convenience, in terms of the gravitational potential Ψ, which can be directly related to $\delta_{(a)}$ through Poisson's equation (see the Appendix).

An isocurvature perturbation, as indicated by its name, corresponds to a perturbation for which the gravitational potential perturbation is zero (or approximately zero). To get a nontrivial isocurvature perturbation, one must therefore have several components and at least one nonvanishing entropy perturbation $S_{A,B}$. For N species, there will be one adiabatic mode and $N-1$ independent isocurvature modes (there is also the possibility to have velocity-type isocurvature modes; see [18]). It is to be noticed that the adiabatic or isocurvature character of perturbations is not time invariant. In the cosmological context, when one talks about adiabatic or isocurvature perturbations, one implicitly assumes that this property corresponds to the *initial* state of the perturbations, which means deep in the radiation era when the wavelength of the perturbation was much larger than the Hubble radius.

In the following, we shall consider primordial perturbations which are hybrid, i.e., which are a sum of adiabatic and isocurvature modes. In order to simplify the exploration of the parameter space, we will restrict our attention to the case of perturbations for which all entropy perturbations within three of the species are zero whereas the last species, X, say, departs from adiabaticity. This means that three of the four species will satisfy the above relation (4) while the contrast density for the remaining species X will be written in the form

$$\frac{\delta_X}{1+w_X} = S_X + \delta_{(a)}, \tag{5}$$

an expression which defines the isocurvature perturbation S_X associated with the species X. Varying X, one can construct four hybrid perturbations of this type.

III. CORRELATIONS

In cosmology, perturbations are treated as homogeneous and isotropic random fields. It is convenient to deal with them in Fourier space rather than ordinary space, and all quantities defined previously can be transformed into their Fourier components, according to the relation (since we work only in flat space)

$$f_{\mathbf{k}} = \int \frac{\mathrm{d}^3\mathbf{x}}{(2\pi)^{3/2}} e^{-i\mathbf{k}\cdot\mathbf{x}} f(\mathbf{x}). \tag{6}$$

Primordial perturbations are usually assumed to be Gaussian, in which case their statistical properties can be summarized simply in terms of their power spectrum, defined for a quantity f by

$$\langle f_{\mathbf{k}} f^*_{\mathbf{k}'} \rangle = 2\pi^2 k^{-3} \mathcal{P}_f(k)\, \delta(\mathbf{k}-\mathbf{k}'). \tag{7}$$

When primordial perturbations are described by *several quantities*, such as would be the case if one has a mixture of adiabatic and isocurvature perturbations, one can also define, for any pair of random fields f and g, a *covariance spectrum* $\mathcal{C}_{f,g}(k)$ by the following expression:

$$\Re\langle f_{\mathbf{k}} g^*_{\mathbf{k}'} \rangle = 2\pi^2 k^{-3} \mathcal{C}_{f,g}(k)\, \delta(\mathbf{k}-\mathbf{k}'). \tag{8}$$

The correlation between f and g can also be expressed in terms of a *correlation spectrum* $\tilde{\mathcal{C}}_{f,g}(k)$ obtained by normalizing $\mathcal{C}_{f,g}(k)$:

$$\tilde{\mathcal{C}}_{f,g}(k) = \frac{\mathcal{C}_{f,g}(k)}{\sqrt{\mathcal{P}_f(k)}\sqrt{\mathcal{P}_g(k)}}. \tag{9}$$

In the present work, we are especially interested in the possible correlation between adiabatic and isocurvature primordial perturbations, i.e., $\tilde{\mathcal{C}}_{\Phi,S}(k)$. Until very recently, only independent mixtures, i.e., with vanishing correlation, were considered in the literature. This statistical independence means that the quantities Φ and S can be expressed as

$$\Phi = \mathcal{P}_\Phi^{1/2} e_1, \quad S = \mathcal{P}_S^{1/2} e_2, \tag{10}$$

where e_1 and e_2 are *independent* normalized centered Gaussian random fields [i.e., such that $\langle e_i(\mathbf{k})\rangle = 0$, $\langle e_i(\mathbf{k}) e_j^*(\mathbf{k}')\rangle = \delta_{ij}\delta(\mathbf{k}-\mathbf{k}')$, for $i,j=1,2$], and where the subscript $\mathbf{k}$ is implicit, as will be the case in the rest of this paper. With the assumption (10), one obtains immediately vanishing covariance and correlation spectra.

However, as was shown in a specific model of double inflation [10], one can also envisage models of the early universe where *correlated* primordial perturbations are generated. To be more specific, this would be the case if one imagines several independent stochastic processes taking place in the early universe, which contribute *both* to adiabatic and isocurvature perturbations, i.e., such that

$$\Phi = \sum_i \Phi_i e_i, \quad S = \sum_i S_i e_i, \tag{11}$$

where the e_i are *independent* normalized centered Gaussian random fields. In the specific example of [10], there were two independent random fields, generated by the quantum fluctuations of two scalar fields.

In the present article, our goal will be to study systematically the consequences of a *totally correlated mixture* of adiabatic and isocurvature perturbations, i.e., primordial perturbations which can be written in terms of one *single* random field. Of course, the consequences of more general initial conditions can then be obtained by simply adding the spectra (to get the total density power spectrum or the total temperature fluctuation multipole spectrum) of several totally correlated initial conditions.

IV. LONG WAVELENGTH ANALYSIS

As shown in the Appendix, it is possible to solve analytically the evolution of the long wavelength perturbations. Totally correlated perturbations can be defined by two primordial quantities: the gravitational potential perturbation deep in the radiation era, denoted $\hat{\Phi}$, and the entropy perturbation, denoted S_X (the index X depends on the species which departs from adiabaticity as explained in Sec. II). It is then possible, using the expressions of the Appendix, to compute observational quantities at the time of last scattering as functions of the two primordial quantities $\hat{\Phi}$ and S_X *for scales larger than the Hubble radius at the time of last scattering*.

In this section, we will use, instead of the energy density contrasts δ_A defined previously in the longitudinal gauge (1), the slightly redefined energy density contrasts (defined in the flat-slicing gauge)

$$\begin{aligned} &\Delta_\gamma = \delta_\gamma - 4\Psi, \quad \Delta_\nu = \delta_\nu - 4\Psi, \\ &\Delta_b = \delta_b - 3\Psi, \quad \Delta_c = \delta_c - 3\Psi. \end{aligned} \tag{12}$$

The reason to use these quantities is essentially that the conservation equations look much simpler (see the Appendix). Moreover, it is to be noticed that, with these new density contrasts, the definitions of adiabatic and isocurvature fluctuations keep exactly the same form. In other words, a purely adiabatic perturbation, as defined by Eq. (4), will also be characterized by

$$\Delta_b = \Delta_c = \frac{3}{4}\Delta_\nu = \frac{3}{4}\Delta_\gamma \equiv \Delta_{(a)}. \tag{13}$$

For a mixed perturbation, with the species X deviating from adiabaticity, the same relation will hold for the three species other than X, and the density of the latter will be given by

$$\frac{\Delta_X}{1+w_X} = S_X + \Delta_{(a)}. \tag{14}$$

Our purpose will now be to express the observable quantities for long wavelength modes, namely, the gravitational potential in the matter era and the temperature anisotropies, in terms of the primordial quantities $\hat{\Phi}$ and S_X. This will be possible by using the two following relations, which are demonstrated in the Appendix. The first relation gives the metric perturbation in terms of the primordial density contrast, during the radiation era,

$$\begin{aligned} \Phi_{\rm rad} \equiv \hat{\Phi} = -\frac{1}{4}\left(3+\frac{4}{5}\Omega_\nu^{\rm RD}\right)^{-1}\Bigg[2\left(1-\frac{4}{5}\Omega_\nu^{\rm RD}\right)\Omega_\gamma^{\rm RD}\Delta_\gamma \\ + \frac{2}{5}(9-4\Omega_\nu^{\rm RD})\Omega_\nu^{\rm RD}\Delta_\nu\Bigg], \end{aligned} \tag{15}$$

the second one being the analogous equation during the matter era:

$$\Phi_{\rm matter} = -\frac{1}{5}(\Omega_b^{\rm MD}\Delta_b + \Omega_c^{\rm MD}\Delta_c). \tag{16}$$

Note that, in the above equations, $\Omega_\nu^{\rm RD}$ and $\Omega_\gamma^{\rm RD}$ are taken in the radiation era, whereas $\Omega_b^{\rm MD}$ and $\Omega_c^{\rm MD}$ correspond to their values in the matter era.

Our hybrid perturbations can be specified either by the pair $(\hat{\Phi}, S_X)$ or the pair $(\Delta_{(a)}, S_X)$, the relation between the two following immediately from the relation (15). For a purely adiabatic perturbation, it is easy to see, using Eq. (15), that

$$\Delta_{(a)} = -\frac{3}{2}\left(3 + \frac{4}{5}\Omega_\nu^{\rm RD}\right)\hat{\Phi} \equiv \alpha\hat{\Phi}. \tag{17}$$

For a mixed perturbation, there will be in general an additional term proportional to S_X. In the case of the baryons and CDM, the expression for $\Delta_{(a)}$ is the same as the adiabatic case, simply because Δ_b and Δ_c do not appear in Eq. (15). For the relativistic species, one obtains

$$\begin{aligned}\Delta_{(a)} &= -\frac{3}{2}\left(3 + \frac{4}{5}\Omega_\nu^{\rm RD}\right)\hat{\Phi} - \left(1 - \frac{4}{5}\Omega_\nu^{\rm RD}\right)\Omega_\gamma^{\rm RD} S_\gamma \\ &\equiv \alpha\hat{\Phi} + \beta_\gamma S_\gamma \end{aligned} \tag{18}$$

for a photon-type hybrid perturbation and

$$\begin{aligned}\Delta_{(a)} &= -\frac{3}{2}\left(3 + \frac{4}{5}\Omega_\nu^{\rm RD}\right)\hat{\Phi} - \frac{1}{5}(9 - 4\Omega_\nu^{\rm RD})\Omega_\nu^{\rm RD} S_\nu \\ &\equiv \alpha\hat{\Phi} + \beta_\nu S_\nu \end{aligned} \tag{19}$$

for a neutrino-type hybrid perturbation.

Substituting in Eq. (16) the expressions of Δ_b and Δ_c in terms of $\Delta_{(a)}$ and S_X, thus in terms of $\hat{\Phi}$ and S_X, it is then possible to find the gravitational potential perturbation during the matter era. For a purely adiabatic perturbation, one finds

$$\Phi_{\rm adiab} = \frac{3}{10}\left(3 + \frac{4}{5}\Omega_\nu^{\rm RD}\right)\hat{\Phi}. \tag{20}$$

One recognizes the standard transfer coefficient of 9/10 if one ignores the anisotropic pressure of neutrinos (see, e.g., [19]). Here, we have its generalization, which is numerically very close to 1, when the anisotropic pressure is taken into account. For a hybrid perturbation, the gravitational potential perturbation during the matter era will be of the form

$$\Phi = \Phi_{\rm adiab} + \Phi_{\rm isoc}, \tag{21}$$

where $\Phi_{\rm adiab}$ corresponds to the term proportional to $\hat{\Phi}$, which is, in all cases, given by the same expression (20), and $\Phi_{\rm isoc}$ is the term proportional to S_X, whose explicit expression depends on the particular species considered. For baryons and CDM, its form is simply

$$\Phi_{\rm isoc} = -\frac{1}{5}\Omega_X^{\rm MD} S_X, \quad X = b, c. \tag{22}$$

For a photon-type mixed perturbation, one finds

$$\Phi_{\rm isoc} = \frac{1}{5}\left(1 - \frac{4}{5}\Omega_\nu^{\rm RD}\right)\Omega_\gamma^{\rm RD} S_\gamma, \tag{23}$$

and finally, for a neutrino-type hybrid perturbation, one gets

$$\Phi_{\rm isoc} = \frac{1}{25}(9 - 4\Omega_\nu^{\rm RD})\Omega_\nu^{\rm RD} S_\nu. \tag{24}$$

The decomposition (21) expresses the fact that a primordial isocurvature perturbation will also contribute, *in the matter era*, to the potential perturbation, whereas it is of course not the case in the radiation era. This illustrates, once more, that the separation between adiabatic and isocurvature modes is not conserved during the time evolution.

Let us now evaluate the contribution of the primordial perturbations to the CMB temperature anisotropies, here only for large angular scales since we are restricted to long wavelength perturbations. Neglecting a local monopole and dipole contribution, the temperature anisotropies, due to scalar perturbations, are approximatively given by (see [20,21])

$$\frac{\Delta T}{T} = \frac{1}{4}\Delta_{\gamma\rm LSS} + (\Phi + \Psi)_{\rm LSS} - e^i \partial_i (V_{\rm LSS}) + \int_{\eta_{\rm LSS}}^{\eta_0} (\dot{\Phi} + \dot{\Psi}) {\rm d}\lambda, \tag{25}$$

where e^i is a spatial unit vector corresponding to the direction of observation, the subscript LSS indicates that the quantities are evaluated at the last scattering surface, an overdot denotes derivation with respect to the conformal time η, η_0 is today's conformal time, and the integral in the last term runs on the photon line of sight. The contribution due to the first two terms is usually called the Sachs-Wolfe (SW) term, while the third term is called the Doppler term and the last one the integrated Sachs-Wolfe (ISW) term. In general, but not always (see the pathological cases below), the SW term is dominant for large angular scales. In terms of our variables, the SW term can be written

$$\left(\frac{\Delta T}{T}\right)_{\rm SW} = \frac{1}{4}\Delta_\gamma + \Phi + \Psi \simeq \frac{1}{4}\Delta_\gamma + 2\Phi, \tag{26}$$

where the quantities are evaluated at the last scattering surface, assuming that last scattering occurs well in the matter era (in this case $\Psi \simeq \Phi$). Using the expressions obtained above, it is now possible to express the SW term as a function of the primordial perturbations $\hat{\Phi}$ and S_X. As for the gravitational potential perturbation, one can decompose this term into

$$\left(\frac{\Delta T}{T}\right)_{\rm SW} = \left(\frac{\Delta T}{T}\right)_{\rm adiab} + \left(\frac{\Delta T}{T}\right)_{\rm isoc}, \tag{27}$$

where the adiabatic component is the term proportional to $\hat{\Phi}$ and the isocurvature component is proportional to S_X. For all types of hybrid perturbations, the adiabatic term is the same:

$$\left(\frac{\Delta T}{T}\right)_{\rm adiab} = \frac{1}{10}\left(3+\frac{4}{5}\Omega_\nu^{\rm RD}\right)\hat{\Phi}. \tag{28}$$

Note that one has $\Delta T/T_{\rm adiab}=\Phi_{\rm adiab}/3$, which is reminiscent of the standard (adiabatic) Sachs-Wolfe term. As for the isocurvature term, it will depend on the particular type of perturbation. For hybrid perturbations which are baryon or CDM isocurvature, one finds

$$\left(\frac{\Delta T}{T}\right)_{\rm isoc} = -\frac{2}{5}\Omega_X^{\rm MD} S_X, \quad X=b,c. \tag{29}$$

Note that, for baryons and CDM, one has the relation $(\Delta T/T)_{\rm isoc}=2\Phi_{\rm isoc}$, and by comparison with the similar relation for the adiabatic terms, one recognizes the standard statement in the literature that pure isocurvature perturbations (of the baryon or CDM type) produce large scale temperature fluctuations *6 times bigger* than pure adiabatic perturbations. For the photon isocurvature hybrid perturbation, one will get

$$\left(\frac{\Delta T}{T}\right)_{\rm isoc} = \frac{1}{15}\left[6-\frac{9}{5}\Omega_\nu^{\rm RD}+\frac{4}{5}(\Omega_\nu^{\rm RD})^2\right]S_\gamma, \tag{30}$$

whereas, for the neutrino isocurvature hybrid perturbation, the expression is

$$\left(\frac{\Delta T}{T}\right)_{\rm isoc} = \frac{1}{75}(9-4\Omega_\nu^{\rm RD})\Omega_\nu S_\nu. \tag{31}$$

V. NUMERICAL ANALYSIS

The present section will be devoted to predictions of temperature anisotropies, as well as the large scale structure power spectrum, for primordial correlated hybrid adiabatic and isocurvature perturbations. We will keep fixed a certain number of parameters, $\Omega_\Lambda=0$, $\Omega_0=1$, $h_{100}=0.5$, $\Omega_b=0.05$; three species of massless nondegenerate neutrinos (leading to $\Omega_\gamma^{\rm RD}=1/[1+(21/8)(4/11)^{4/3}]\simeq 0.595$ and $\Omega_\nu^{\rm RD}=1-\Omega_\gamma^{\rm RD}\simeq 0.405$); and standard recombination. The primordial perturbations will be assumed to be scale invariant.

A. Temperature anisotropies

As far as temperature anisotropies are concerned, isocurvature perturbations can be distinguished from pure isocurvature perturbations by a much larger plateau, as explained in the previous section, with the consequence that all the acoustic peaks will appear smaller than this plateau. To show these two extreme behaviors we have plotted in Fig. 1 the case of pure adiabatic initial conditions and, in Fig. 2, the case of pure CDM-type isocurvature initial conditions. We have also plotted, in each case, the SW, Doppler, and ISW

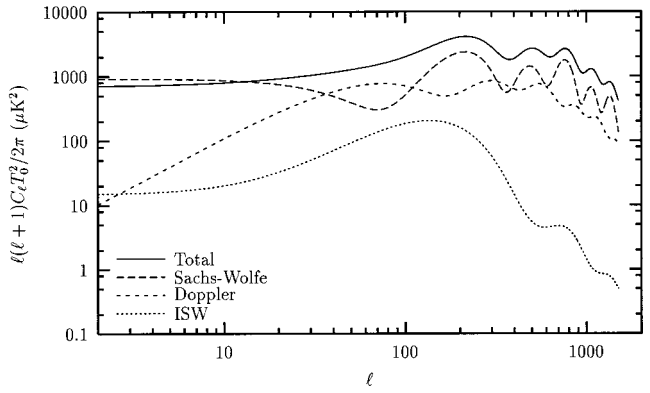

FIG. 1. CMB anisotropies in the pure adiabatic model ($\lambda=0$). The solid line represents the total (scalar) contribution. The Sachs-Wolfe, Doppler, and integrated Sachs-Wolfe contributions are, respectively, represented by long-dashed, short-dashed, and dotted lines. At large angular scales (low l), the total amplitude is essentially due to the Sachs-Wolfe contribution.

contributions. We have used, as usual, the angular power spectrum for the temperature anisotropies, defined by

$$C_l^{TT}=\langle |a_{lm}^T|^2\rangle, \tag{32}$$

where the a_{lm}^T are the multipole coefficients that appear in the decomposition into spherical harmonics of the temperature fluctuations, i.e.,

$$\frac{\Delta T}{T}=\sum_{l,m} a_{lm}^T Y_{lm}. \tag{33}$$

In the case of hybrid perturbations, we will be somehow between these two extreme situations. For convenience, let us parametrize the hybrid perturbations by λ, which is defined by the relation

$$S=\lambda\hat{\Phi}, \tag{34}$$

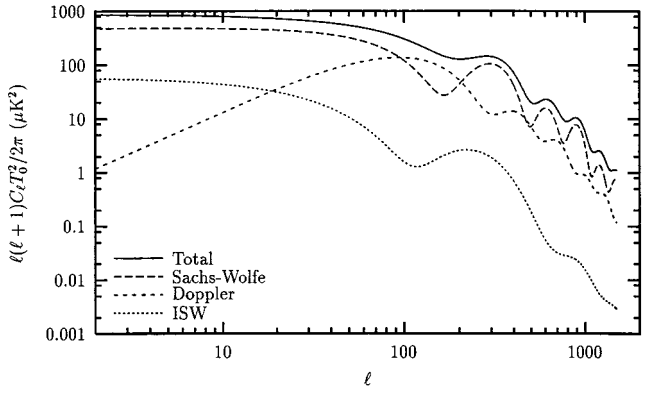

FIG. 2. CMB anisotropies in the pure isocurvature CDM model ($\lambda=\pm\infty$). The solid line represents the total scalar contribution. The Sachs-Wolfe (SW), Doppler, and integrated Sachs-Wolfe contributions are, respectively, represented by long-dashed, short-dashed, and dotted lines. Note that the power at large scales (low l) is higher than at the degree scale.

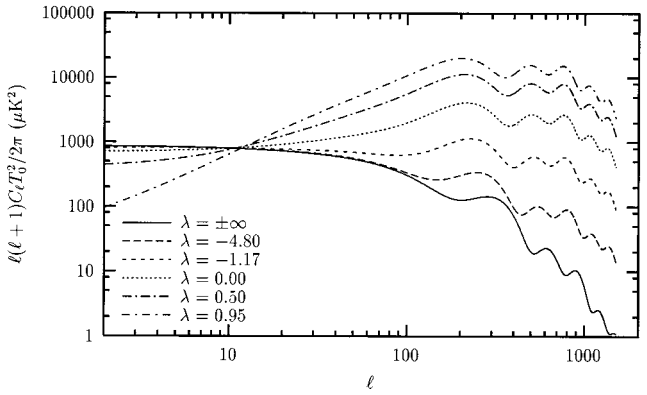

FIG. 3. CMB anisotropies in CDM-type correlated hybrid models for various values of the parameter λ. The highest curve is studied in more detail in Fig. 8, the dotted curve represents the (standard) adiabatic case, and the lowest represents the pure isocurvature case shown in Fig. 2. Note that the height of the acoustic peaks with respect to the Sachs-Wolfe plateau varies with λ, according to Eq. (42).

and which will quantify how far we are from a purely adiabatic model. The case $\lambda=0$ corresponds to pure adiabatic initial conditions, whereas the limit where λ goes to infinity corresponds to pure isocurvature perturbations. λ can be positive or negative. To be more specific, one can call the hybrid perturbations we are studying *correlated* when $\lambda>0$ and *anticorrelated* when $\lambda<0$. In Figs. 3–5, we have plotted the total temperature anisotropy as a function of the multipole index l for various values of the parameter λ (for CDM-type hybrid perturbations) and keeping the same normalization at large angular scales.

To emphasize the difference between correlated hybrid perturbations and independent hybrid perturbations, which have been considered in the literature, we have plotted, in Fig. 6, the total temperature anisotropy for independent hybrid initial conditions. The curves are parametrized by the number $\mathcal{R}$, which is defined by

$$\mathcal{P}_S^{1/2}=\mathcal{R}\mathcal{P}_\Phi^{1/2}. \tag{35}$$

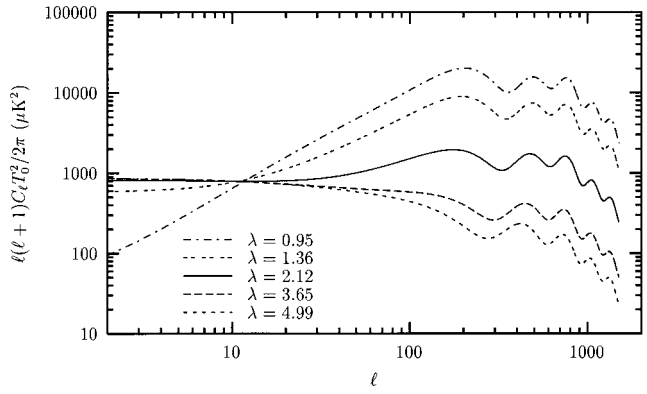

FIG. 4. CMB anisotropies in CDM-type correlated hybrid models for various values of the parameter λ. The two highest curves are studied in more details in Figs. 7 and 8.

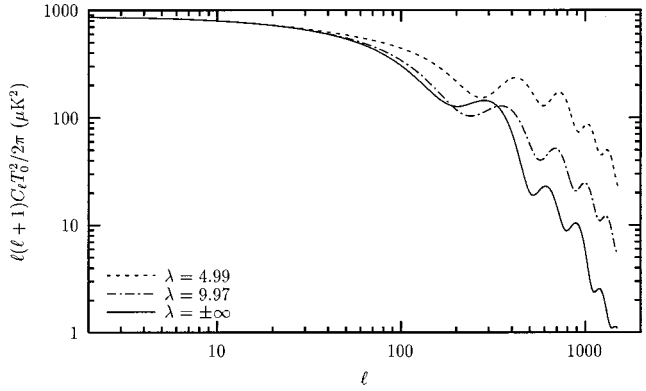

FIG. 5. CMB anisotropies in CDM-type correlated hybrid models for large (positive) values of the parameter λ. The solid curve represents the pure isocurvature case of Fig. 2. Note that the height of the acoustic peaks with respect to the Sachs-Wolfe plateau varies slowly in this range of values for λ.

In some sense $\mathcal{R}$ is the analogue, in the independent case, of λ since the square of both quantities corresponds to the ratio of the power spectra. But of course $\mathcal{R}$ can be only positive. The way these curves are obtained is also different. Whereas for the correlated mixtures one implements hybrid initial conditions from the beginning and one runs the Boltzmann code once (per model), in the case of independent mixtures one runs the code first with purely adiabatic initial conditions, then a second time with purely isocurvature initial conditions, and the final C_l are obtained by a weighted sum of the C_l obtained from each run. As a consequence, the first acoustic peak, as well as the subsequent ones, will always appear lower, relative to the plateau, in the hybrid case than in the purely adiabatic case.

The behavior of the C_l for the correlated hybrid models is quite different when one increases the isocurvature proportion. For anticorrelated perturbations, i.e., $\lambda<0$, the behavior is what is expected naively: the amplitude of the peaks de-

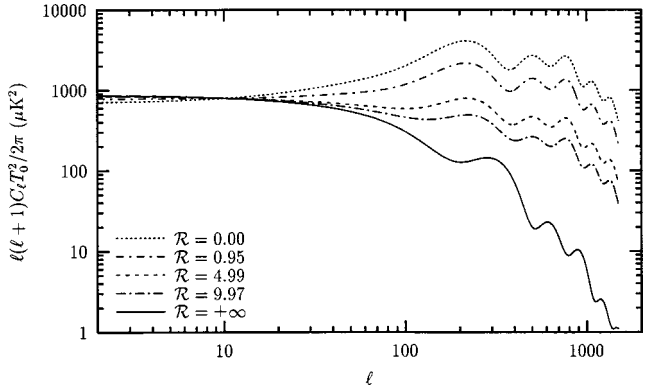

FIG. 6. CMB anisotropies in independent (uncorrelated) hybrid CDM-type models for various values of the parameter $\mathcal{R}$. The lowest, solid curve represents the pure isocurvature case of Fig. 2 ($\mathcal{R}=\infty$), and the highest, dotted curve represents the adiabatic case ($\mathcal{R}=0$). We have chosen for $\mathcal{R}$ the same numerical values as for λ in Figs. 3–5. Note the significant difference between the correlated and the independent cases especially in the region where $\mathcal{R},\lambda\simeq 1$.

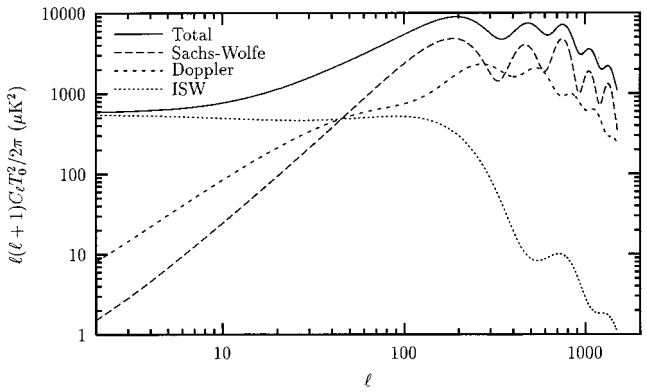

FIG. 7. CMB anisotropies in a CDM-type correlated hybrid model (with $\lambda=1.36$). The solid line represents the total (scalar) contribution. The Sachs-Wolfe (SW), Doppler, and integrated Sachs-Wolfe contributions are, respectively, represented by long-dashed, short-dashed, and dotted lines. The parameter λ has been chosen so that the SW contribution cancels at lowest order. In this case, the low multipole power is no longer dominated by the SW contribution, but rather by the ISW contribution.

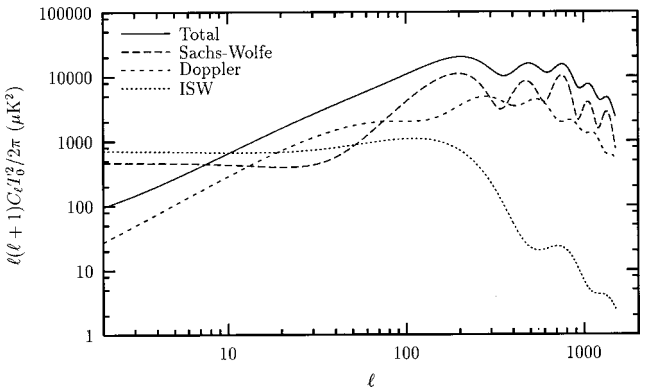

FIG. 8. CMB anisotropies in a CDM-type correlated hybrid model (with $\lambda=0.95$). The solid line represents the total contribution. The Sachs-Wolfe (SW), Doppler, and integrated Sachs-Wolfe (ISW) contributions are, respectively, represented by long-dashed, short-dashed, and dotted lines. The parameter λ has been chosen so that the SW and ISW contributions almost cancel each other at lowest order. In this case, the low multipole power is dominated by the Doppler contribution, which is not flat at low multipoles.

creases, relative to the plateau, with a higher proportion of isocurvature perturbations, as illustrated in Fig. 3, with the curves lower than the adiabatic case. But the evolution is more complicated when one considers correlated models, i.e., with $\lambda>0$. Starting from the adiabatic case ($\lambda=0$) and increasing λ slowly, one begins with a phase where the amplitude of the peaks will increase with respect to the plateau, as illustrated by the curves above the adiabatic one in Fig. 3. If one goes on increasing λ, one reaches a critical value, beyond which the peaks will now diminish with increasing λ, as illustrated by the curves of Fig. 4.

One can understand this surprising behavior if one goes back to the results of the previous section. In the case of CDM hybrid perturbations, one can evaluate the SW plateau, using Eqs. (28) and (29),

$$\left(\frac{\Delta T}{T}\right)_{\rm SW}=\left[\frac{1}{10}\left(3+\frac{4}{5}\Omega_\nu^{\rm RD}\right)-\frac{2}{5}\Omega_c^{\rm MD}\lambda\right]\hat{\Phi}, \qquad (36)$$

and therefore there is indeed a critical value for λ for which the SW plateau is suppressed, which explains the relative height of the peaks. In fact, things are slightly more complicated, because when the SW term is suppressed, due to this special choice of initial conditions, the other terms which contribute to the anisotropies cannot be neglected any longer. Figure 7 shows in particular that the plateau can be due essentially to the ISW effect. Note that the value $\lambda=1.36$ for which this effect was numerically obtained is slightly different from the value one would deduce from Eq. (36). This is because Eq. (36) was obtained by supposing that the last scattering surface is completely in the matter-dominated era, which is not the case since the radiation-to-matter transition occurs not very long before recombination. One can also adjust the initial conditions so that the large scale anisotropies will be dominated by the Doppler term, in which case there is no longer a plateau on large scales, but an increasing slope as can be seen in Fig. 8.

Although at this stage we have discussed and illustrated only the CDM correlated hybrid case, a similar behavior appears for the three other types of correlated hybrid perturbations, but with noticeable differences. We have systematically explored the parameter space for the four types of correlated hybrid initial conditions and measured the predicted height of the first acoustic peak with respect to the plateau. The results are given in Fig. 9. Here, we have adopted a different parametrization of the hybrid correlated perturbations so that one can represent easily all cases. We have defined an angular variable θ_X so that our initial conditions for the density contrasts are of the form

$$\frac{\Delta_X}{1+w_X}=\cos\theta_X, \quad \frac{\Delta_A}{1+w_A}=\sin\theta_X, \quad A\neq X, \qquad (37)$$

which implies

$$S_X=(\cot\theta_X-1)\Delta_{(a)}. \qquad (38)$$

Of course, this parameter θ_X can be related to the parameter λ. Let us write

$$\Delta_{(a)}=\alpha\hat{\Phi}+\beta_X S_X, \qquad (39)$$

where the subscript X for the coefficient β_X refers to the type of hybrid mode we are considering. α is the same for all four types and is given by the coefficient in Eq. (17). β_X is zero for the CDM and baryon modes and is given by the second term on the right hand side in Eqs. (18) and (19) for the photon and neutrino cases, respectively. The relation between λ_X and θ_X is then

$$\lambda_X=\frac{(\cot\theta_X-1)\alpha}{1-(\cot\theta_X-1)\beta_X}. \qquad (40)$$

In the region near $\theta=\pi/4$ (corresponding to the pure adiabatic case and where all curves cross), it is easy to see that

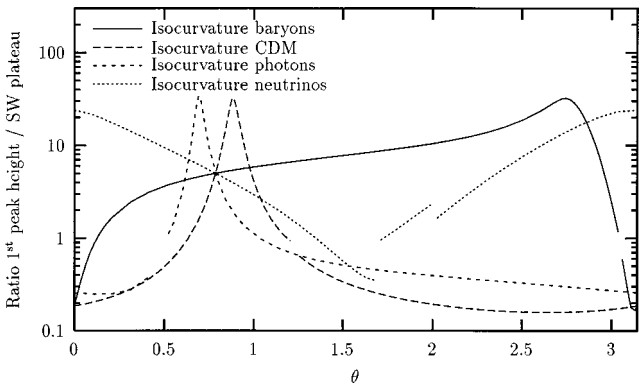

FIG. 9. Ratio of the height of the first acoustic peak to the height of the Sachs-Wolfe (SW) plateau for the four types of hybrid models. The height of the SW plateau is obtained by averaging the power between $l=2$ and $l=25$, which correspond to the angular scales explored by COBE. We have defined the ''first acoustic peak'' as the first maximum of the multipole anisotropy spectrum for $l \geqslant 100$. Each ratio peaks at a high value ($\simeq 30$) which roughly corresponds to the moment where the SW plateau disappears [see Eq. (42); in practice, this occurs when the SW and ISW contributions cancel at low multipoles]. The four curves intersect at $\theta = \pi/4$, as expected, since this value corresponds to the pure adiabatic case [see Eq. (38)]. As θ varies, the position on the l axis of the first acoustic peak slightly shifts to the left or to the right (see also Fig. 10). In some cases, the peak goes below $l=100$. In this case the ''new'' first acoustic peak position is at $l \simeq 200$–300, and its height is different, hence the discontinuities in the curves.

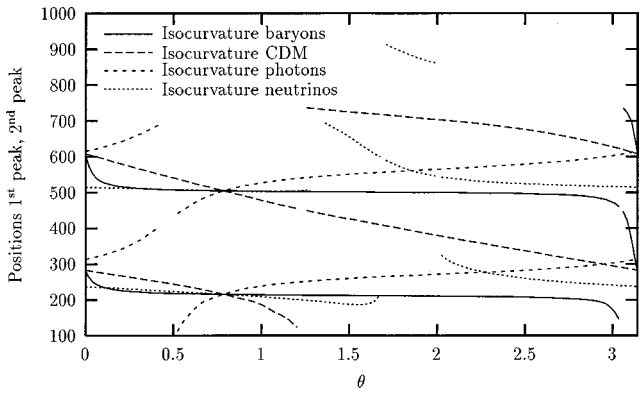

FIG. 10. Position of the two first acoustic peaks in the four types of hybrid models. As explained in Fig. 9, the first acoustic peak is defined as the first maximum of the multipole anisotropy spectrum for $l \geqslant 100$. In some cases ($\theta \simeq 3$ for the isocurvature baryon model, $\theta \simeq 0.5$ for the isocurvature photon model, and $\theta \simeq 1.2$ for the isocurvature CDM model), the first peak disappears in the low multipole region, and the ''new'' first peak becomes the ''former'' second one. In some other cases, the peaks is smeared in the power spectrum and disappears, as is the case for the first acoustic peak in the isocurvature neutrino model at $\theta \simeq 1.2$ and at $\theta \simeq 1.7$ for the second one.

the relation between θ and λ is the same for the four types of perturbations and is given numerically by

$$\lambda \simeq 2\alpha(\theta - \pi/4) \simeq 9.97(\theta - \pi/4). \tag{41}$$

Let us see what happens when one deviates from the pure adiabatic case. In the baryon case, the first peak will increase for correlated mixtures and decrease for anticorrelated mixtures, as in the CDM case, although in a much more moderate way. On the contrary, in the photon and neutrino cases, the first peak will start to increase for *anticorrelated* perturbations. Moreover, the evolution in the neutrino case is slower than in the photon case.

All these results can be understood rather easily with the analytical results of the previous section. Indeed, in all cases, the SW anisotropy term can be written in the form

$$\left(\frac{\Delta T}{T}\right)_{\mathrm{SW}} = (a + b_X \lambda_X)\hat{\Phi}, \tag{42}$$

where the special case of CDM is given just above. The coefficient a is the same for all four cases, as was shown in the previous section. Therefore, the evolution of the SW plateau will be determined by the coefficient b_X which is different in each case. For baryon and CDM perturbations, the coefficient b is negative, which explains why the increase of the first peak (or equivalently the decrease of the plateau) corresponds to correlated ($\lambda > 0$) perturbations when one deviates from the pure adiabatic case. Moreover, $|b_c| > |b_b|$ because $\Omega_c > \Omega_b$ and therefore the response to the increase of the isocurvature proportion is stronger in the CDM case. In the photon and neutrino cases, the coefficient β is positive and therefore only anticorrelated perturbations can lead to an increase of the peak. Moreover, $b_\gamma > b_\nu$, and similarly to the heavy species, the response to the increase of λ is stronger in the photon case than in the neutrino case. A consequence of these results is that, potentially, the correlated hybrid perturbations in the CDM and photon cases will be more strongly constrained by the CMB measurements than the baryon and neutrino cases.

It is also important, in the spirit of putting constraints on this type of modes, to see the position of the two Doppler peaks on the l axis. We have plotted in Fig. 10 the positions of the first and second acoustic peaks. Near the pure adiabatic case, the behavior is once more strongly pronounced in the CDM and photon cases. In this region, in the CDM case, correlated hybrid perturbations tend to displace the peaks to smaller l whereas anticorrelated perturbations push the peaks to higher l. The same behavior, but very attenuated, seems to apply to the baryon and neutrino cases. In contrast, in the photon case, higher l correspond to correlated perturbations and lower l to anticorrelated perturbations.

Another important feature of the acoustic peaks is the impact of the isocurvature part on the amplitude of the second peak. Figure 11 gives the evolution of the relative amplitude of the second peak with respect to the first peak, when one varies the coefficient λ, for the four types of perturbations. As before, in the vicinity of the pure adiabatic point, the effects are more important in the CDM and photons cases than in the two other cases.

B. Power spectrum

In the previous subsection, we have analyzed the CMB fluctuations. Another important part of the observational data

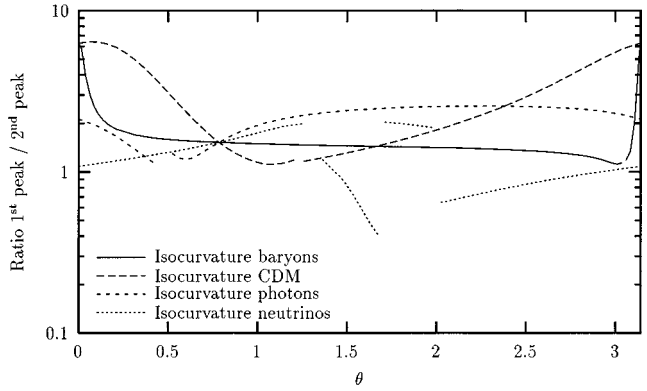

FIG. 11. Relative heights of the first two acoustic peaks for the four types of hybrid models. The various discontinuities of the four curves originate from the discontinuities in the peak positions, explained and illustrated in Fig. 10.

comes from the large scale structures. However, it is more difficult to infer precise information from the large scale structure data as from the expected CMB measurements, because of additional complications such as the bias effect. Moreover, the signatures due to pure adiabatic perturbations and pure isocurvature perturbations, respectively, are easier to distinguish in the CMB anisotropies than in the matter power spectrum. But nevertheless the LSS power spectrum is a useful tool, at least to check the overall amplitude of the perturbations.

To illustrate the power spectra corresponding to correlated hybrid perturbations, we have plotted in Figs. 12–14, the power spectra (taking the gravitational potential perturbation as reference variable) in the case of CDM-type correlated hybrid perturbations, for various values of λ.

Some interesting behavior occurs for large values of λ. When $\lambda \geqslant \alpha$, it is easy to see using Eq. (40) that the CDM and the baryon density contrasts have initially opposite signs. The CDM density contrast evolves [see Eqs. (A1),(A2)] according to the equation

$$\ddot{\Delta}_c + \mathcal{H}\dot{\Delta}_c = -k^2\Phi, \tag{43}$$

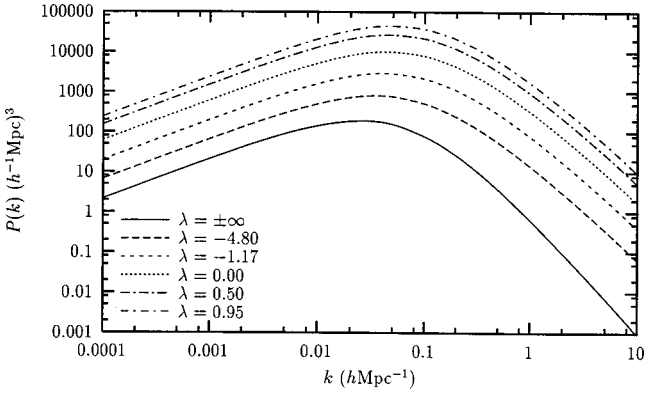

FIG. 12. Matter power spectra in the CDM-type hybrid models for various values of the parameter λ. All the curves have been normalized to COBE. Note that the overall amplitude, as well as the position of the maximum, varies with λ.

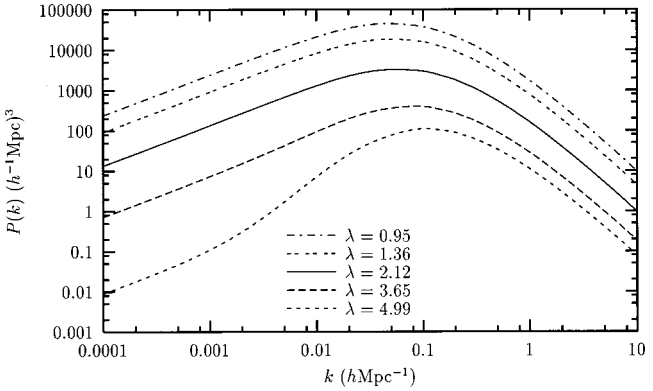

FIG. 13. Matter power spectra in the CDM-type hybrid models for various values of the parameter λ. All the curves have been normalized to COBE.

which can be solved to give

$$\Delta_c = \Delta_c^{\text{init}} - k^2 \int \left[\frac{1}{a} \int a\Phi \, \mathrm{d}\eta \right] \mathrm{d}\eta', \tag{44}$$

where Δ_c^{init} is the initial value for the CDM density contrast, so that it will evolve towards values with sign opposite to that of Φ, that is, of the same sign as $\Delta_{(a)}$. Moreover, the shortest wavelengths will evolve rapidly enough and change sign whereas the longest wavelengths will not, so that the CDM power spectrum should exhibit a sign change. For a given mode, this sign change occurs all the more rapidly as the initial CDM density contrast is small as compared to $\hat{\Phi}$, that is, when λ is small. Plotting the matter power spectrum, it is therefore natural to expect that the wave number at which it is zero is all the more small as λ is small. This is what we can check in Fig. 14.

C. CMB polarization

Although CMB polarization has not yet been measured and is expected to be difficult to measure, it can provide a lot of additional information concerning the cosmological perturbations and the cosmological parameters [22]. This is why

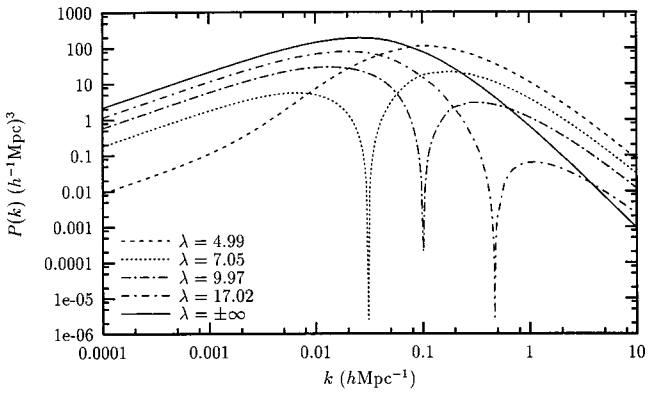

FIG. 14. Matter power spectra in the CDM-type hybrid models for high values of the parameter λ. All the curves have been normalized to COBE. Note that one the power spectrum goes to zero for a critical scale, which depends on the value of λ.

we will consider briefly the consequence of correlated hybrid perturbations on the CMB polarization. The polarization can be decomposed [22] into *E*-mode polarization and *B*-mode polarization, and we shall define, in addition to the temperature angular power spectrum, the *E*-mode angular power spectra

$$C_l^{EE} \equiv \langle |a_{lm}^E|^2 \rangle \tag{45}$$

and the correlation spectrum

$$C_l^{ET} \equiv \langle a_{lm}^{T*} a_{lm}^E \rangle, \tag{46}$$

where the a_{lm}^T correspond here to the same coefficients as those defined in Eq. (33), which gives the correlation between the temperature and the *E*-mode polarization. Scalar-type perturbations do not contribute to the *B*-mode polarization. As an illustration, we have plotted the *E*-mode polarization anisotropy spectrum for various values of λ. Two features in these curves are obvious. First, the amplitude of the polarization varies, as well as the position of the first peak in the spectrum. This can be understood by looking at the Boltzmann equation for the photon fluid. Before the last scattering surface, Thomson diffusion is important, and the photon anisotropic stress approximatively obeys the equation

$$\sigma_\gamma \simeq -\frac{4}{15}\frac{k}{\dot{\kappa}} V_{b\gamma}, \tag{47}$$

where $\dot{\kappa}$ stands for the differential Thomson opacity, and $V_{b\gamma}$ is the photon-baryon plasma velocity. Thus, the photon anisotropic stress [which is proportional to the *E*-type polarization; see Eqs. (62), (63), (77) of [23]] is proportional to the photon dipole, and the C_l^{EE} are proportional to the Doppler contribution of the CMB temperature anisotropy spectrum. Therefore, the position and height of the peaks vary for both spectra in the same way with λ. These results are represented in Fig. 15 and the cross-correlation spectrum between temperature and polarization can be found in Fig. 16.

VI. CONCLUSION

In the present work, our goal has been to analyze the effects of correlated hybrid adiabatic and isocurvature perturbations on observational quantities, in particular the CMB anisotropies. We have isolated four ''elementary'' modes, corresponding to a deviation from adiabaticity of one of the four standard species (photons, neutrinos, baryons, CDM): each type of these elementary modes is characterized by only two parameters (S and $\Delta_{(a)}$). One could, of course, generalize our analysis by relaxing the adiabatic ratios among the three remaining species, but at the price of requiring four parameters.

We have shown, in the case of these elementary modes, that correlation leads to very specific effects on the CMB anisotropies and on large scale structure which do not appear in the case of independent mixtures.

In this paper, our purpose was not to directly confront observations with this type of model, but rather to focus on some qualitative interesting consequences of correlated hybrid perturbations. This is why we have considered only a subclass of models, which are extreme in the sense that they are totally correlated and simple because they are described by only two parameters. If one wishes to compare hybrid models with observations, one should consider the *sum* of spectra of the type we have obtained (as explained in Sec. III), which means that the adiabatic and isocurvature perturbations would then be only partially correlated (this is the case in the specific model of [10]).

The present data are still too imprecise to be able to distinguish this kind of correlated hybrid perturbation, but it may be interesting to know how much precise data would constrain these modes. In practice, it might turn out to be a

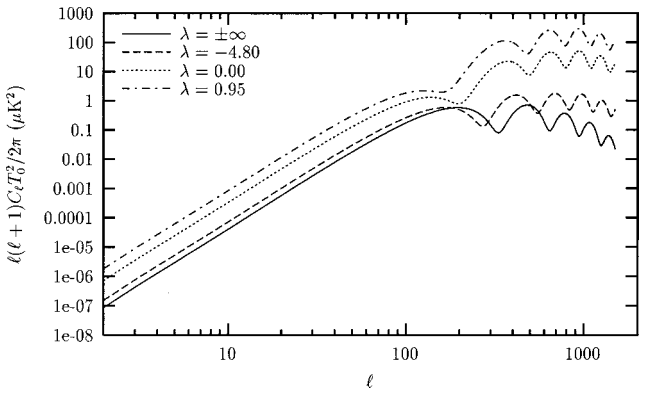

FIG. 15. CMB polarization anisotropies in the CDM-type hybrid models for various values of the parameter λ. We have represented the spectrum for the same values of λ as in Fig. 3 (but we have omitted two of them for clarity). The amplitude of the spectrum decreases and the peaks shift to the right as one goes from the adiabatic case (λ = 0, dotted line) to the pure isocurvature case (λ = ±∞, solid line), as the spectrum closely follows that of the Doppler contribution to the temperature anisotropy spectrum (see Figs. 1 and 2).

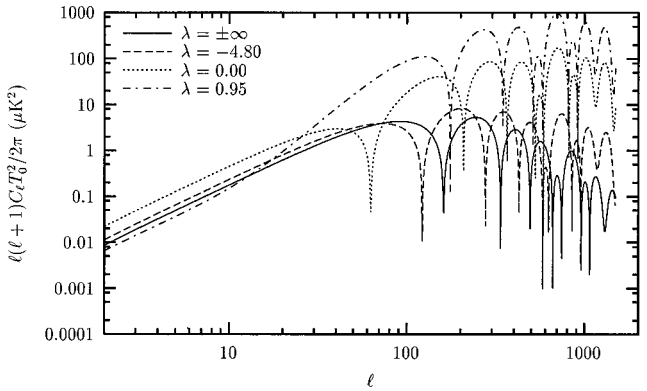

FIG. 16. CMB temperature-polarization cross-correlation spectrum in the CDM-type hybrid models for various values of the parameter λ. As in Fig. 15, we have represented the spectrum for the same values of λ as in Fig. 3 and have omitted two of them for clarity. The amplitude of the spectrum decreases and the peaks shift to the right as one goes from the adiabatic case (λ = 0, dotted line) to the pure isocurvature case (λ = ±∞, solid line).

difficult task to disentangle the presence of such modes in the data, unless one assumes a specific early universe model.

ACKNOWLEDGMENTS

It is a pleasure to thank Nabila Aghanim, Francis Bernardeau, Martin Bucher, Kavilan Moodley, and David Spergel for interesting discussions.

APPENDIX: EVOLUTION OF PERTURBATIONS

In this appendix, we derive the evolution of all quantities for long wavelengths, i.e., *scales outside the Hubble radius*: $k \ll aH$. The whole system of equations, in a notation slightly different from the one adopted here, can be found, for example, in [24].

Let us first introduce the system of equations governing the evolution of the matter perturbations, which relate the density contrasts of the four species to the scalar component of their velocities (denoted by V_A). We first have four equations of conservation, one for each of the four species, which read (in Fourier space)

$$\begin{aligned}
\dot{\Delta}_\nu &= \frac{4}{3} k V_\nu, \\
\dot{\Delta}_c &= k V_c, \\
\dot{\Delta}_\gamma &= \frac{4}{3} k V_{b\gamma}, \\
\dot{\Delta}_b &= k V_{b\gamma},
\end{aligned} \tag{A1}$$

where a prime denotes a derivative with respect to the conformal time η and where $V_{b\gamma}$ is the velocity common to the baryon and photon fluids, which are coupled until last scattering. We then have three Euler equations, two for the independent fluids of CDM and neutrinos, and one for the baryon-photon fluid:

$$\begin{aligned}
\dot{V}_\nu &= -k\left[\frac{\Delta_\nu}{4} + \Psi + \Phi - \sigma_\nu\right], \\
\dot{V}_c &= -\mathcal{H} V_c - k\Phi, \\
\dot{V}_{b\gamma} &= -\frac{3\Omega_b}{4\Omega_\gamma + 3\Omega_b}\mathcal{H} V_{b\gamma} \\
&\quad - k\frac{4\Omega_\gamma}{4\Omega_\gamma + 3\Omega_b}\left[\frac{\Delta_\gamma}{4} + \Psi\right] - k\Phi,
\end{aligned} \tag{A2}$$

where $\mathcal{H}$ is the comoving Hubble parameter defined by $\mathcal{H} \equiv a'/a$. In the last equation, the coefficients Ω_A are time dependent since the ratio of the energy density of a given species with respect to the critical energy density, will change with time.

To close the above system of equations, one needs the Einstein equations, which express the metric perturbations in terms of the matter perturbations. Only two components of the Einstein equations are useful, the other ones being redundant, and they are the Poisson equation,

$$-\left[\frac{k^2}{\mathcal{H}^2} + \frac{9}{2}(1+w)\right]\Psi = \frac{3}{2}\sum_X \Omega_X\left[\Delta_X - \frac{3\mathcal{H}}{k}(1+w_X)V_X\right], \tag{A3}$$

and the anisotropic stress equation,

$$\frac{k^2}{\mathcal{H}^2}(\Psi - \Phi) = 6\Omega_\nu \sigma_\nu, \tag{A4}$$

where σ_ν represents the anisotropic stress due to the neutrinos (which thus require a description beyond the perfect fluid approximation). To get the evolution of σ_ν, one must use a higher moment of the Boltzmann equation (see [24]),

$$\dot{\sigma}_\nu = -\frac{4}{15} k V_\nu, \tag{A5}$$

where other terms on the right hand side have been neglected.

In order to solve the above equations for long wavelengths, it is convenient to consider an expansion of all quantities in terms of the small parameter $k\eta$, so that one will have

$$X = X^{(0)} + X^{(1)} k\eta + X^{(2)} (k\eta)^2 + \cdots. \tag{A6}$$

The Euler equations (A2) then enable us to express the first order velocity term as a function of the zeroth order density and gravitational potentials:

$$\begin{aligned}
V_\nu^{(1)} &= -\frac{1}{4}\Delta_\nu^{(0)} - \Psi^{(0)} - \Phi^{(0)}, \\
V_c^{(1)} &= -\frac{\Phi^{(0)}}{1 + \mathcal{H}\eta}, \\
V_{b\gamma}^{(1)} &= -\frac{\Omega_\gamma \Delta_\gamma^{(0)} + 4\Omega_\gamma \Psi^{(0)} + (4\Omega_\gamma + 3\Omega_b)\Phi^{(0)}}{4\Omega_\gamma + 3(1+\mathcal{H}\eta)\Omega_b}.
\end{aligned} \tag{A7}$$

The zeroth order components of the velocities are as usual set to zero; otherwise, one would get a divergence on the right hand side of Eq. (A3) (unless there is a special cancellation of the type mentioned in [18]).

Using Eqs. (A4) and (A5) at lowest order, one gets

$$\Psi^{(0)} - \Phi^{(0)} = -\frac{4}{5}\Omega_\nu \mathcal{H}^2 \eta^2 V_\nu^{(1)}, \tag{A8}$$

and substituting the above expression for $V_\nu^{(1)}$, one finds the following relation between $\Phi^{(0)}$ and $\Psi^{(0)}$:

$$\left(1 + \frac{4}{5}\Omega_\nu \mathcal{H}^2 \eta^2\right)\Phi^{(0)} = \left(1 - \frac{4}{5}\Omega_\nu \mathcal{H}^2 \eta^2\right)\Psi^{(0)} - \frac{1}{5}\Omega_\nu \mathcal{H}^2 \eta^2 \Delta_\nu^{(0)}. \tag{A9}$$

Substituting in Poisson's equation (A3), at lowest order, the expressions obtained above for the velocities, and using Eq. (A9), one finally gets the following cumbersome equation, relating $\Phi^{(0)}$ to the four species densities:

$$-\left\{(3+\Omega_\gamma+\Omega_\nu)\left(1+\frac{4}{5}\Omega_\nu y^2\right)+\frac{(4\Omega_\gamma+3\Omega_b)y}{4\Omega_\gamma+3\Omega_b(1+y)}\left[8\Omega_\gamma+3\Omega_b\left(1-\frac{4}{5}\Omega_\nu y^2\right)\right]+\frac{3y}{1+y}\Omega_c\left(1-\frac{4}{5}\Omega_\nu y^2\right)\right.$$
$$\left.+8y\Omega_\nu\right\}\frac{\Phi^{(0)}}{1-\frac{4}{5}\Omega_\nu y^2}$$
$$=\Omega_b\Delta_b^{(0)}+\Omega_c\Delta_c^{(0)}+\frac{4\Omega_\gamma(1+y)+3\Omega_b(1+2y)}{4\Omega_\gamma+3\Omega_b(1+y)}\Omega_\gamma\Delta_\gamma^{(0)}+\left[\frac{4}{5}\Omega_\gamma y^3\frac{4\Omega_\gamma+3\Omega_b}{4\Omega_\gamma+3\Omega_b(1+y)}\right.$$
$$\left.+1+y+(3+\Omega_\gamma-3\Omega_\nu)\frac{y^2}{5}\right]\frac{\Omega_\nu\Delta_\nu^{(0)}}{1-\frac{4}{5}\Omega_\nu y^2}, \tag{A10}$$

where $y\equiv\mathcal{H}\eta$. While this expression yields the evolution of the gravitational potential perturbation during the whole evolution of the universe from the deep radiation era until the last scattering, it will be sufficient for our present purpose to retain from this equation only its asymptotic forms in the radiation era and the matter era. In the radiation era, $y=1$ and $\Omega_c,\Omega_b \ll\Omega_\gamma,\Omega_\nu$, so that the above expression simplifies to give

$$\Phi^{(0)}=-\frac{1}{4}\left(3+\frac{4}{5}\Omega_\nu\right)^{-1}\left[2\left(1-\frac{4}{5}\Omega_\nu\right)\Omega_\gamma\Delta_\gamma^{(0)}+\frac{2}{5}(9-4\Omega_\nu)\Omega_\nu\Delta_\nu^{(0)}\right]. \tag{A11}$$

In the matter era, $y=2$ and $\Omega_\gamma,\Omega_\nu\ll\Omega_c,\Omega_b$, so that one finds

$$\Phi^{(0)}=-\frac{1}{5}(\Omega_b\Delta_b^{(0)}+\Omega_c\Delta_c^{(0)}). \tag{A12}$$

[1] http://map.gsfc.nasa.gov
[2] http://astro.estec.esa.nl/SA-general/Projects/Planck
[3] R. Stompor, A. J. Banday, and K. M. Gorski, Astrophys. J. **463**, 8 (1996).
[4] M. Kawasaki, N. Sugiyama, and T. Yanagida, Phys. Rev. D **54**, 2442 (1996).
[5] S. D. Burns, astro-ph/9711303.
[6] A. A. de Laix and R. J. Scherrer, Astrophys. J. **464**, 539 (1996).
[7] T. Kanazawa, M. Kawasaki, N. Sugiyama, and T. Yanagida, Prog. Theor. Phys. **102**, 71 (1999).
[8] K. Enqvist and H. Kurki-Suonio, Phys. Rev. D **61**, 043002 (2000).
[9] E. Pierpaoli, J. Garcia-Bellido, and S. Borgani, J. High Energy Phys. **10**, 015 (1999).
[10] D. Langlois, Phys. Rev. D **59**, 123512 (1999).
[11] A. D. Linde, Phys. Lett. **158B**, 375 (1985); L. A. Kofman, Phys. Lett. B **173**, 400 (1986); L. A. Kofman and A. D. Linde, Nucl. Phys. **B282**, 555 (1987).
[12] G. Efstathiou and J. R. Bond, Mon. Not. R. Astron. Soc. **218**, 103 (1986).
[13] K. Enqvist and J. McDonald, Phys. Rev. Lett. **83**, 2510 (1999).
[14] A. D. Linde and V. Mukhanov, Phys. Rev. D **56**, 535 (1997).
[15] D. Polarski and A. A. Starobinsky, Phys. Rev. D **50**, 6123 (1994).
[16] P. J. E. Peebles, Nature (London) **327**, 210 (1987); Astrophys. J., Lett. Ed. **315**, L73 (1987).
[17] W. Hu, E. Bunn, and N. Sugiyama, Astrophys. J. **447**, 59 (1995).
[18] M. Bucher, K. Moodley, and N. Turok, astro-ph/9904231.
[19] A. R. Liddle and D. H. Lyth, Phys. Rep. **231**, 1 (1993).
[20] R. K. Sachs and A. M. Wolfe, Astrophys. J. **147**, 73 (1967).
[21] M. Panek, Phys. Rev. D **34**, 416 (1986).
[22] M. Zaldarriaga and U. Seljak, Phys. Rev. D **55**, 1830 (1997).
[23] W. Hu and M. White, Phys. Rev. D **56**, 596 (1997).
[24] C. P. Ma and E. Bertschinger, Astrophys. J. **455**, 7 (1995).